IEEE Access
Multidisciplinary | Rapid Review | Open Access Journal

Received June 24, 2021, accepted July 8, 2021, date of publication July 13, 2021, date of current version July 22, 2021.

*Digital Object Identifier 10.1109/ACCESS.2021.3096972*

# Optimization of Piezoelectric Sensor-Actuator for Plate Vibration Control Using Evolutionary Computation: Modeling, Simulation and Experimentation

**ASAN G. A. MUTHALIF[1], (Senior Member, IEEE), KHAIRUL A. M. NOR[2], AZNI NABELA WAHID[2], AND ABDELRAHMAN ALI[1]**

[1]Department of Mechanical and Industrial Engineering, College of Engineering, Qatar University, Doha, Qatar
[2]Smart Structures, Systems, and Control Research Laboratory, Department of Mechatronics Engineering, International Islamic University Malaysia, Kuala Lumpur 53100, Malaysia

Corresponding author: Asan G. A. Muthalif (drasan@qu.edu.qa)

This work was supported in part by the Qatar University International Research Collaboration under Grant IRCC-2020-017.

**ABSTRACT** The development of lightweight, stronger, and more flexible structures has received the utmost interest from many researchers. For this reason, piezoelectric materials, with their inherent electromechanical coupling, have been widely incorporated in the development of such structures to attenuate their vibrations. However, one of the main challenges is to find the optimal control and sensor-actuator placement. This paper presents an active vibration control for flexible structures, whereby a simply supported plate is taken as the benchmark model. A feedback controller with a collocated sensor-actuator configuration is used. Both disturbance and control signal acting on the plate is created by using piezoelectric (PZT) patches. The analytical model is derived based on the Euler-Bernoulli model. The Optimal location of the collocated sensor-actuator, as well as PID controller gains, are determined using Ant Colony Optimization (ACO) technique, then compared with the Genetic Algorithm (GA) and enumerative method (EM). Optimization in this paper is based on minimizing frequency average energy. The optimal performance value of piezoelectric patch sensor-actuator position and PID controller gains are verified experimentally. It was found that PID controller gains and collocated sensor-actuator location optimizations using ACO, GA and enumerative methods give similar results, which implies the effectiveness of ACO as an optimization technique. More than 20 % of attenuation achieved using the available hardware setup.

**INDEX TERMS** Active vibration control, ant colony optimization, generic algorithm, modeling and simulation, optimization of sensor-actuator location, piezoelectric.

## I. INTRODUCTION

Lighter, stronger, and more flexible structures are said to be the ideal forms of structures in vibration suppression with minimum power consumption [1]. In recent years, the development of lightweight yet stronger structures that can withstand vibrational loads has gained the utmost attention by researchers. Such structures can be developed when piezoelectric patches (sensor-actuator) are integrated with an optimized active vibration control (AVC) strategy [2]. In the advancement of such smart structures, piezoelectrics have shown great promise. Piezoelectric materials can generate an electrical voltage when subjected to mechanical strains and stresses, and vice versa. Under the application of electrical voltage, these materials can generate mechanical strain in response to the applied voltage. Hence, allowing them to be utilized as both sensors and actuators when placed on flexible structures. Piezoelectric actuators have shown significant benefits in vibration control due to their ability to excite only the structures' elastic modes without exciting the rigid body modes. It is crucial since it is often required to control the structures' elastic motions [3].

The continuous nature of the structures has provided flexibility to the placement of the piezoelectric patches on

The associate editor coordinating the review of this manuscript and approving it for publication was Yingxiang Liu.

the structures. To achieve optimal performance, one must ensure the optimal location of the piezoelectric sensor-actuator. Many researchers have investigated the optimal placement of the piezoelectric sensors and actuators on structures. Caruso *et al*. [4] investigated the optimal placement of the actuators and sensors for collocated flexible plates, and the optimal locations were achieved by maximizing the modal controllability and observability of the structure. Hongwei *et al*. [5] have investigated the actuators' optimal locations in a smart structure using optimal control theory. Using the input energy correlation, it was concluded that size, location and control gain were independent of the initial conditions. Bruant and Proslier [6] considered the optimal location of actuators and sensors in the AVC of structures while considering the residual modes to limit spillover effects. By minimizing the linear quadratic regulator cost, Kumar and Narayanan [7] were able to optimize the piezoelectric actuators' location on steel plates. Darivandi *et al.* [8] applied a subgradient-based algorithm to optimize the location of piezoelectric actuators on flexible structures that have been much more efficient and accurate than genetic algorithm optimization. Liu *et al.* [9] have investigated the optimal placements of piezoelectric actuators on structures and demonstrated that particle swarm optimization's computational efficiency is higher than that of the genetic algorithm. Prion *et al.* [10] developed a criterion concerning the optimal placement of a collocated sensor-actuator pair of AVC structures based on the maximization of the pole-zero distance in open-loop, which correlates with the maximum achievable damping ratio in closed-loop. Contero-Chinchilla *et al.* [11] optimized the sensor/actuator placement for structural health monitoring using an objective function that combines parameters uncertainty, expected information entropy and the cost of both sensors and actuators.

Optimal sensor-actuator positions and gains used in the controller are vital to enhancing the performance of a control system and numerous works using conventional optimization techniques such as H (infinity) norm [12], linear quadratic regulator (LQR) [13], and H2 norms [14], were proposed to cope with such problem. Various conventional optimization techniques have been employed for this purpose. However, biologically inspired optimization techniques have shown great potential in optimizing the sensor/actuator location and controller gains of AVC systems Optimization of sensor and/or actuator location and controller gains in AVC system were successfully carried out through biologically-inspired optimization techniques, including particle swarm optimization (PSO) [14], artificial neural network (ANN) [16] and genetic algorithm (GA) [17]–[19]. In 1992, another bio-inspired optimization method based on swarm intelligence, namely Ant Colony Optimization (ACO), was founded. Since then, it has been successfully implemented [20]. The ant colony optimization ACO technique is another bio-inspired method that can be successfully implemented. Furthermore, ACO has shown great potential as an optimization technique due to its simplicity and efficiency. Nevertheless, even with its simplicity, it is shown that attempts using ACO in optimizing the location of the sensor-actuator and controllers for the AVC system is still considerably low. ACO was used to optimally tune the Proportional-Integral-Derivative (PID) controller [21], but these were tested only on arbitrary plants. Hardware-in-the-loop (HIL) optimization with the help of a continuous ant colony system (TCACS) suggested by Nobahari *et al.* [22], to optimize controller and observer parameters for a beam was conducted successfully. Mohamad *et al.* [23], proposed SISO control of a flexible beam using continuous ACO ($ACO_R$).

This paper presents theoretical and experimental works on AVC strategy on a simply supported thin plate using a piezoelectric patch for modal overlap factor (MOF) less than 1. The individual vibration modes distinct, which is equivalent to a frequency range of 0 to 200 Hz. Optimization sensor-actuator location and controller gains are carried out utilizing the ACO and later verified using GA. Using ACO offers simplicity, less complexity and yields a similar level of accuracy. Although many algorithms can be used, this study focused on ACO and GA algorithms. These bio-inspired computing optimizing algorithm has gained interest as it is a promising approach, that can be further developed for new and robust competing techniques. The values obtained from ACO and GA are compared with the enumerative method (the actual value) with objective function as total energy reduction. The purpose of this study is to demonstrate the effectiveness of ACO as an optimization technique.

This paper is organized as follows. Section 2 presents the equation of motion (EOM) of the system. Section 3 explains the optimization algorithms used in this research, i.e., ACO and GA. Section 4 discusses the simulation results for optimal controller gains and sensor-actuator location. Section 5 presents the experimental verification of the optimal parameters found in Section 4.

## II. PLANT MODEL

In this section, the system's equation of motion of the simply supported thin rectangular plate with attached piezoelectric patches for excitation and control is derived. The time-averaged plate energy *EP* is then derived and used in the objective function used for the optimization. The mathematical model of the simply supported plate with piezoelectric patches is derived using the Euler-Bernoulli model; which limits the simulation results to thin plates only. Lagrange's method is employed to derive the equation of motion of a simply supported plate with attached piezoelectric patches.

Consider a simply-supported thin rectangular plate of length $a$, width $b$ and thickness $h$ is taken for this study. Piezoelectric patches were used for excitation and control forces. For linear isotropic material, the constitutive equation of piezoelectric as the actuator is [24]:

$$\sigma = c^E \varepsilon - eE \tag{1}$$

where $\sigma$ is the stress vector, e is the dielectric permittivity matrix, $c^E$ is the matrix of elastic coefficients under constant

electric field, $\varepsilon$ is the strain vector, $E = V(t)/t_p$ is the electric field vector, $V(t)$ is the voltage supplied to the piezoelectric actuator, $t_p$ is the piezoelectric patch thickness. The spatial deflection of the simply supported plate during vibration can be represented as the summation of modes in double series [25]:

$$w(x,y) = \sum_m \sum_n W_{mn} sin\frac{m\pi x}{a} sin\frac{n\pi y}{b} \tag{2}$$

where $W_{mn}$ is the magnitude, and m and n refer to the half-wave number in the $x$ and $y$ directions, respectively. The natural frequency $(m,n)^{th}$ of the plate can be written as:

$$\omega_{mn} = \sqrt{\frac{D}{\rho}}\left[\left(\frac{m\pi}{L_x}\right)^2 + \left(\frac{n\pi}{L_y}\right)^2\right] \tag{3}$$

where $D$ is the flexural rigidity, $\rho$ is the plate density, $L_x$ and $L_y$ refer to the dimensions in the $x$ and $y$ directions.

The potential energy U and kinetic energy T are given by [26]:

$$\begin{aligned} U = {} & \frac{D}{2}\iint\left\{\left(\frac{\partial^2 w}{\partial x^2} + \frac{\partial^2 w}{\partial y^2}\right)^2 - 2(1-v)\right. \\ & \times\left.\left[\left(\frac{\partial^2 w}{\partial x^2}\frac{\partial^2 w}{\partial y^2}\right) - \left(\frac{\partial^2 w}{\partial x \partial y}\right)^2\right]\right\} dA \\ & + \frac{1}{2}\iint D_1(x,y)\left\{\left(\frac{\partial^2 w}{\partial x^2} + \frac{\partial^2 w}{\partial y^2}\right)^2 - 2(1-v)\right. \\ & \times\left.\left[\left(\frac{\partial^2 w}{\partial x^2}\frac{\partial^2 w}{\partial y^2}\right) - \left(\frac{\partial^2 w}{\partial x \partial y}\right)^2\right]\right\} dA \\ & + \frac{1}{2}\iint D_2(x,y)\left\{\left(\frac{\partial^2 w}{\partial x^2} + \frac{\partial^2 w}{\partial y^2}\right)^2 - 2\left(1-v_{pz}\right)\right. \\ & \times\left.\left[\left(\frac{\partial^2 w}{\partial x^2}\frac{\partial^2 w}{\partial y^2}\right) - \left(\frac{\partial^2 w}{\partial x \partial y}\right)^2\right]\right\} dA \\ & + B(t)\iint S(x,y)\left[\left(d_{31} + v_{pz}d_{32}\right)\frac{\partial^2 w}{\partial x^2}\right. \\ & + \left.\left(d_{32} + v_{pz}d_{31}\right)\frac{\partial^2 w}{\partial y^2}\right] dA \end{aligned} \tag{4}$$

$$T = \frac{1}{2}\rho h\iint\left(\frac{\partial w}{\partial t}\right)^2 dA + \frac{1}{2}\rho_{pz}t_p\iint\left(\frac{\partial w}{\partial t}\right)^2 S(x,y)\,dA \tag{5}$$

$S(x,y)$ is the product of Heaviside function for a patch on the plate and can be obtained by:

$$\begin{aligned} S(x,y) = {} & [H(x-x_1) - H(x-x_2)] \\ & \times [H(y-y_1) - H(y-y_2)] \end{aligned} \tag{6}$$

The flexural rigidity of the plate is:

$$D = \frac{E}{\left(1-v^2\right)}\left(\frac{h^3}{12} - z_n\frac{h^2}{8}\right) \tag{7}$$

The flexural rigidity of the plate under the patch area is:

$$D_1(x,y) = D_1 S(x,y) = \frac{E}{\left(1-v^2\right)}\left(\frac{h^3}{12} + z_n^2 h\right) S(x,y) \tag{8}$$

and the flexural rigidity of the piezoelectric patch is obtained by:

$$\begin{aligned} & D_2(x,y) \\ & = D_2 S(x,y) \\ & = \frac{E_{pz}}{\left(1-v_{pz}^2\right)} \\ & \quad \times\left(\frac{t_p^3}{3} + \frac{h^2 t_p}{4} + \frac{h t_p^2}{2} - z_n\left(h t_p + t_p^2\right) + z_n^2 t_p\right) S(x,y) \end{aligned} \tag{9}$$

and,

$$B(t) = \frac{E_{pz}V(t)}{2\left(1-v_{pz}^2\right)}\left(h + t_p - 2z_n\right) \tag{10}$$

where $\rho$ and $\rho_{pz}$ are the plate and piezoelectric density, respectively, and $A$ is the plate area. $d_{31}$ and $d_{32}$ are piezoelectric strain constants ($d_{32} = d_{31}$, because of isotropic), E and $E_{pz}$ are Young's modulus for plate and piezoelectric patch. v and $v_{pz}$ is Poisson's ratio for the piezoelectric patch.

The term $z_n$ is the shifted neutral axis measured from the plate center due to the single patch attachment i.e.

$$z_n = \frac{E_{pz}t_p\left(h + t_p\right)}{2\left(Eh + E_{pz}t_p\right)}$$

Substitution of both potential and kinetic energies into Lagrange's Equation produce an equation of motion of the system as:

$$\left(-\omega^2 M + K_C\right) W_{mn} = f_e + f_a \tag{11}$$

where $\omega$ is the angular frequency, $M$ is the mass matrix. By substituting both the derived potential and kinetic energies into the Lagrange's equation, it produces the equation of motion of the system, where the term $(j\eta + 1)K$ is substituted by $K_c$ for simplicity. Where $K$ is the stiffness matrix, and $j$ is an imaginary point. $\eta$ is the modal loss factor, $W_{mn}$ is the vector representing modal amplitude, and $f_e$ and $f_a$ are the modal force vector for exciter and actuator patches, respectively.

PID controller involves feedback signal, its derivative, and it's integral, i.e. the feedback signal is equivalent to velocity term. The mass, stiffness, and damping matrices due to PID controller is denoted by $M_{PID}$, $K_{PID}$ and $C_{PID}$ respectively. The EOM of the system with a PID controller is written as [27]:

$$\left(-\omega^2\left(M + M_{PID}\right) + \left(K_C + K_{PID}\right) + j\omega C_{PID}\right) w_{mn} = f_e \tag{12}$$

the time-averaged plate energy, $EP$, can be calculated from

$$EP = \frac{1}{2} {w_{mn}}^T K_C w_{mn} \tag{13}$$

Thus, the frequency-averaged plate enrgy, $\overline{EP}$, measured from an initial frequency $f_{in}$ to final frequency $f_{fi}$ is:

$$\bar{EP} = \frac{\sum_{f_{in}}^{f_{fi}} EP\,(f)}{f_{fi} - f_{in}} \tag{14}$$

## III. OPTIMIZATION FUNCTION

The objective function used for optimization is defined as:

$$min \frac{1}{ER} = \frac{\overline{EP}_{nc}}{\overline{EP}_{nc} - \overline{EP}_c} \tag{15}$$

where $\overline{EP}_c$ and $\overline{EP}_{nc}$ are the average plate energy with and without control, respectively. This objective function aims to find five optimal parameters: the x- and y-coordinates of sensor-actuator location $(x_{sa}, y_{sa})$ and the $K_p$, $K_i$ and $K_d$ of the PID controller. Optimization of five variables simultaneously is difficult and time-consuming; thus, the process is divided into two [18].

1. Optimize $x_{sa}$ and $y_{sa}$ while considering velocity feedback control with 1000 $Ns/m$, approximately 100 times driving point impedance, as an initial gain.
2. Optimize $K_p$, $K_i$ and $K_d$, using optimal sensor-actuator location found above.

Vibration mode shapes of a flexible structure have nodes and anti-nodes. It is difficult to control the vibration by placing the actuator on a node even with a large actuating force. The location of the sensor-actuator patches is more critical than the PID gains, hence, the PID gains are optimized after finding the optimal sensor-actuator location.

### A. ANT COLONY OPTIMIZATION

In this paper, we utilized Simple-ACO (SACO) algorithm for optimization purpose. Inspired by a colony of ants looking for a food source, the algorithm finds optimal parameter values of any objective function based on the probability equation given by:

$$\mathrm{P_k}\,(\mathrm{t}) = \begin{cases} \frac{\left\{\tau_{\mathrm{ij}}\,(\mathrm{t})\right\}^{\alpha}}{\sum_{\mathrm{i,j}\in \mathrm{T_k}} \left\{\tau_{\mathrm{ij}}\,(\mathrm{t})\right\}^{\alpha}}, & \text{if } j \in T_k \\ 0, & \text{otherwise} \end{cases} \tag{16}$$

where $\tau$ is the pheromone trail mimicking trail made by an ant while searching for food, $t$ is time, $\alpha$ is the relative importance of the pheromone values and $T_k$ does the ant $k$ effectuate the path at a given time. The magnitude of pheromone disposed of by an ant during a tour is represented by:

$$\Delta\tau_{ij}\,(t) = \begin{cases} \frac{Q}{L_k}, & \text{if } (i,j) \text{ walked by ant } k. \\ 0, & \text{otherwise} \end{cases} \tag{17}$$

where Q is a constant and $L_k$ is the cost of tour by ant k or the objective function. In our case, $L_k$ is the inverse of energy reduction calculated using Eq. (13). The next ants follow the trails with more potent pheromones and reinforce it with their pheromone. On the other hand, the weaker pheromone trails will eventually evaporate. Mathematically, this can be represented by:

$$\tau_{ij}\,(t) = \sigma\,\tau_{ij}\,(t-1) + \sum_{k=1}^{NA} \Delta\tau_{ij}\,(t) \tag{18}$$

Forgetfulness of the bad choices are introduced by $\sigma$, the pheromone decay $0 < \sigma < 1$, and $NA$ is the number of ants. ACO parameters used in this paper are given in Table 1.

**TABLE 1. ACO parameters.**

| Parameter | Value |
|---|---|
| Number of ants | 10 |
| Maximum generation | 50 |
| $\alpha$ | 1 |
| Pheromone decay, $\sigma$ | 0.95 |

### B. GENETIC ALGORITHM

GA, a well-established algorithm, is used in this paper to ascertain the results found by ACO method. It is inspired by the natural evolutionary process mechanics and had successfully solved problems involving optimization of actuator location and controller gains [28]–[33]. The GA parameters used in this study are listed in Table 2, and other settings are left to their default value.

**TABLE 2. GA parameters.**

| Parameter | Value |
|---|---|
| Population size | 10 |
| Number of generations | 50 |
| Crossover probability | 0.8 |

Flowcharts of the SACO algorithm is given in Figure 1, and the optimization strategy is illustrated in Figure 2.

The optimal values from both ACO and GA are compared against the enumerative method since it gives the actual optimal point. As the purpose is to reduce modal energy, the exciter should be placed at a single location that can excite the required modes.

## IV. SIMULATION RESULTS

Parameters of the simulation model are given in Table 3. For simulation purpose, the exciter patch is assumed to be located at (0.15 m, 0.15 m), while the control patch with collocated sensor-actuator configuration will be found through optimization. The frequency range of interest is between 0 to 200 Hz, and the resonant frequencies within this range are shown in Table 4.

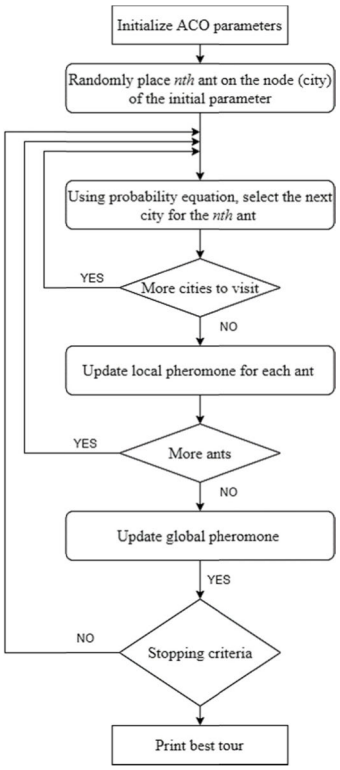


**FIGURE 1.** Flowchart of SACO algorithm.

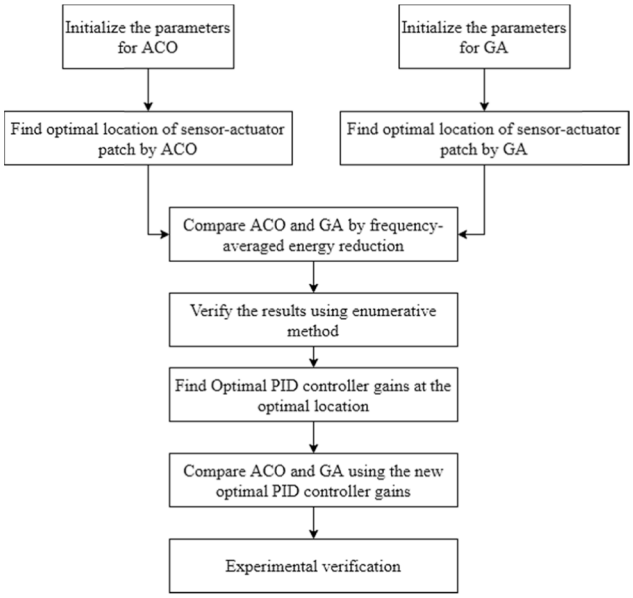


**FIGURE 2.** Optimization strategy.

### A. OPTIMAL SENSOR-ACTUATOR LOCATION

To make the results as precise as possible, 10000 possible values of $x_{sa}$ and 10000 possible values of $y_{sa}$ are used, making the distances between consecutive one-two nodes along the $x$-axis and $y$-axis as $4.5005 \times 10^{-5}$ m and $5.8006 \times 10^{-5}$ m, respectively. Table 5 and Figures 3(a) and 3(b) show optimization results.

**TABLE 3.** Benchmark model.

| Parameter | Plate | Piezoelectric Patch |
|---|---|---|
| Width | $0.6\ m$ | $0.02\ m$ |
| Length | $0.5\ m$ | $0.05\ m$ |
| Density | $8000\ kg/m^3$ | $7750\ kg/m^3$ |
| Thickness | $0.001\ m$ | $0.0001\ m$ |
| Loss factor | 0.05 | 0.05 |
| Poisson's ratio | 0.30 | 0.31 |
| Young's Modulus | $279 \times (10^9\ N)/m^2$ | $70 \times (10^9\ N)/m^2$ |
| Piezoelectric constants, $d_{31}$ and $d_{32}$ | - | $-(19e^{-12}\ C)/N$ |
| Material | Stainless Steel | PZT-5A |

**TABLE 4.** Resonant frequencies less than 200 Hz.

| Mode | Frequency (Hz) |
|---|---|
| 1 | 18.9 |
| 2 | 42.2 |
| 3 | 52.4 |
| 4 | 75.8 |
| 5 | 80.9 |
| 6 | 107.9 |
| 7 | 114.4 |
| 8 | 131.1 |
| 9 | 134.7 |
| 10 | 168.1 |
| 11 | 169.9 |
| 12 | 185.9 |

**TABLE 5.** Optimal position.

| | | *ACO* | *GA* |
|---|---|---|---|
| Variables | $x_{sa}$ | 0.1529 | 0.1562 |
| | $y_{sa}$ | 0.1434 | 0.1491 |
| Energy Reduction (%) | 1st mode | 10.24 | 11.09 |
| | 2nd mode | 19.73 | 20.27 |
| | 3rd mode | 13.30 | 13.64 |
| | 4th mode | 25.37 | 24.76 |
| | 5th mode | 17.22 | 15.70 |
| | Frequency-averaged | 10.06 | 10.13 |

As shown in Table 5, the results from both optimization methods agree to each other. The effect of a negative velocity feedback control to the plate energy is clearly shown in Figure 3(a), whereby the controlled energy plot experiences a significant reduction of amplitude without any natural frequency shifting. The best location to place the sensor-actuator patch is near the exciter patch with more than

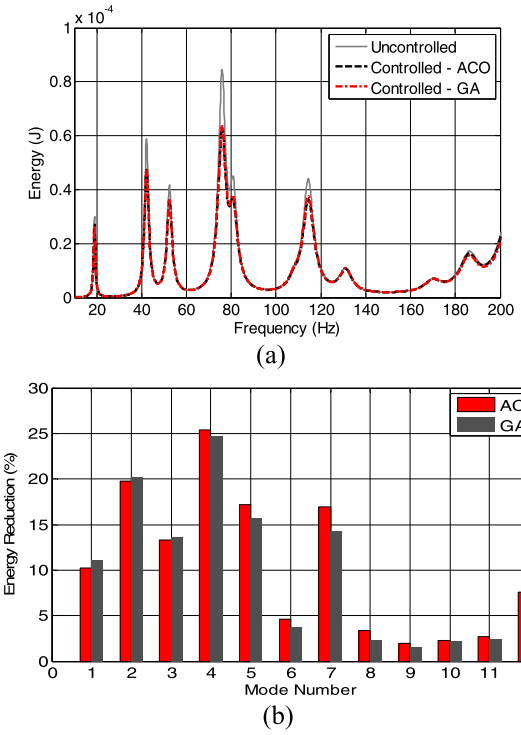


**FIGURE 3.** (a) Plate energy plot and (b) energy reduction for each mode using the optimal location of the sensor-actuator.

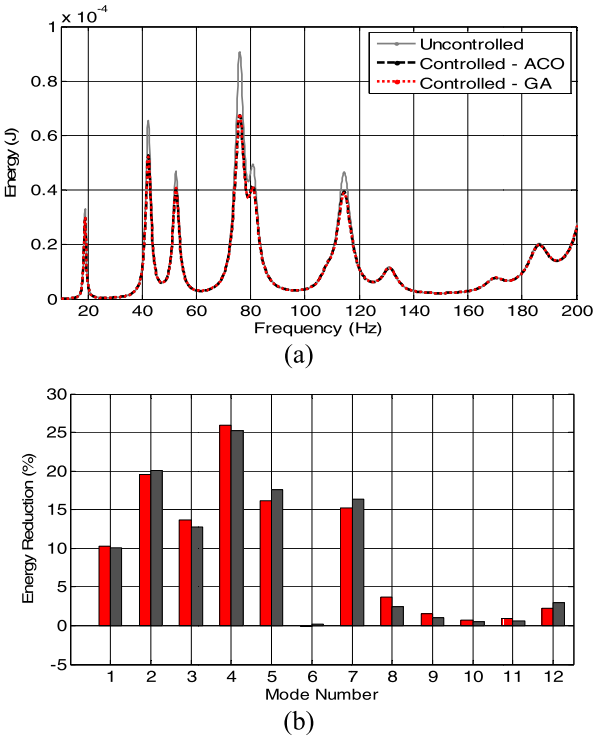


**FIGURE 4.** (a) Plate energy plot and (b) energy reduction for each mode using the revised optimal location of the sensor-actuator.

**TABLE 6.** Revised sensor-actuator location.

| | | *ACO* | *GA* |
|---|---|---|---|
| Variables | $x_{sa}$ | 0.3511 | 0.3472 |
| | $y_{sa}$ | 0.4550 | 0.4594 |
| Energy Reduction (%) | 1st mode | 10.23 | 10.12 |
| | 2nd mode | 19.52 | 20.04 |
| | 3rd mode | 13.71 | 12.79 |
| | 4th mode | 25.91 | 25.25 |
| | 5th mode | 16.12 | 17.56 |
| | Frequency-averaged | 8.29 | 8.32 |

10% frequency-averaged energy reduction. This is because the highest energy reduction can be achieved by directly locking the disturbance force. Nevertheless, the actuator's placement close to the disturbance point is not a practical solution since we normally do not know the location that causes vibration and its corresponding magnitude. Hence, optimal location is searched again by setting at least 0.1 m gabs, along x and y axes, between excitation and sensor-actuator locations. Table 6 shows the result and illustrated in Figures. 4(a) and 4(b). The revised optimal sensor-actuator locations found are at (0.3511 m, 0.4550 m) and (0.3472 m, 0.4592 m) using ACO and GA, respectively.

An enumerative method is used to verify results from GA and ACO. It is a conservative technique in which the sensor-actuator is systematically placed to all grid points of the plate, and its corresponding energy reduction is measured. The accuracy of the result depends on the number of grid points taken for simulation. Even with coarse grid points, this method can predict the optimal location. A 3-D plot describing energy reduction concerning the location of the sensor-actuator is shown in Figure 5. The optimal sensor-actuator locations for first and second highest energy reduction are (0.160 m, 0.155 m) and (0.358 m, 0.4547 m).

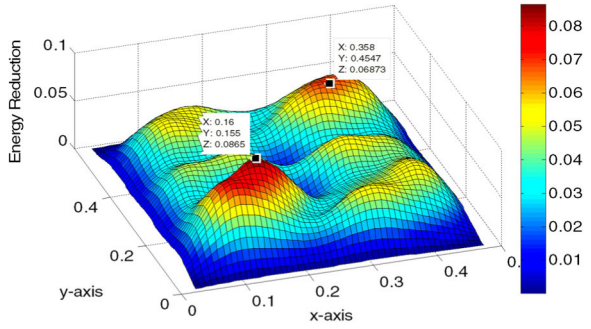


**FIGURE 5.** Energy reduction with different sensor-actuator locations.

### B. OPTIMAL PID CONTROLLER GAINS

The optimal value of $K_p$, $K_i$ and $K_d$ were found when the sensor-actuator was at the optimal location i.e. ($x_{sa} = 0.3511$, $y_{sa} = 0.4550$). The range of values for $K_p$, $K_i$ and $K_d$ considered here are 0 to 1000, 0 to 500 and 0 to 50, respectively.

**TABLE 7. Optimal PID gains.**

| | | *ACO* | *GA* |
|---|---|---|---|
| Variables | $k_p$ | 990 | 911.55 |
| | $k_i$ | 210 | 203.33 |
| | $k_d$ | 19.88 | 20.19 |
| Energy Reduction (%) | 1st mode | 18.86 | 17.66 |
| | 2nd mode | 31.86 | 30.09 |
| | 3rd mode | 24.10 | 22.65 |
| | 4th mode | 40.14 | 38.12 |
| | 5th mode | 25.43 | 23.92 |
| | Frequency-averaged | 24.30 | 23.78 |

Table 7 shows Kp's optimal values, $K_i$ and $K_d$ obtained using ACO and GA and its corresponding energy reduction.

Figure 6(a) shows the PID controller had altered the system's natural frequencies. This was due to the change in mass-stiffness-damping matrices as given in Eq. (12) above. Figure 6(b) shows energy reduction for each mode. It can be seen that the energy of the mode whose frequency is around 110 Hz is increased. However, This is the trade-off done when controlling broadband vibration using a single actuator. The location of the sensor-actuator is chosen so that frequency-average energy is reduced. As such, the optimization algorithm will identify an actuator that optimally applies force on many modes within the bandwidth; this, in turn, may undesirably add energy to some modes. The situation would be different if the aim is to control individual mode, as different actuator location is needed for every mode. When using a piezoelectric patch as an actuator, changing its location is impossible since it is bonded strongly/permanently on the plate. Another option is to use multiple actuators in different locations to target various modes. The current work aims to use a single piezoelectric actuator to target and control many modes optimally.

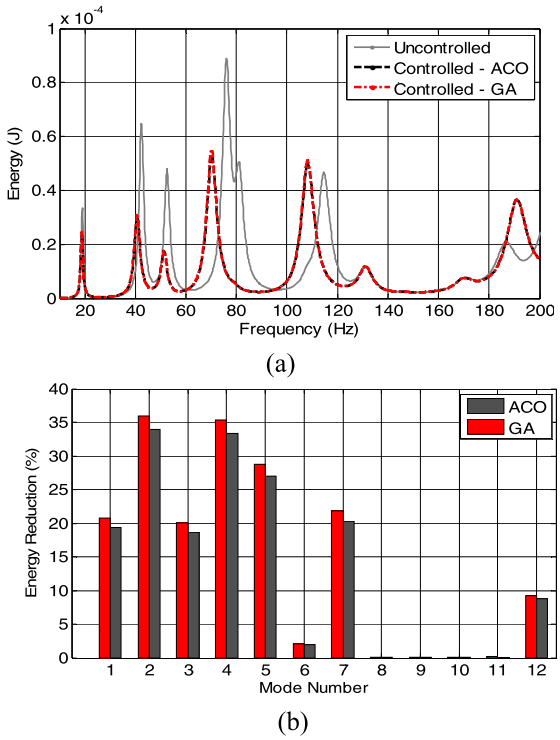


**FIGURE 6. (a) Plate energy and (b) energy reduction for each mode using optimal PID.**

## V. EXPERIMENTAL RESULTS

The experimental setup comprised of a thin stainless-steel plate with a dimension of $0.6\ m \times 0.5\ m \times 0.001\ m$ lying on a frame to mimic a simply supported boundary condition. Vibration excitation and suppression are generated by 2 MIDE piezoelectric patches and each is connected to ACX power amplifier model EL-1225 with 20-time amplification factor. Eight units of PCB accelerometer model 352C33 are used for energy estimation, while another unit located on top of the actuator patch meant for feedback signal purpose. Only one actuator is used to implement the broadband vibration control optimally. The generation of the excitation signal and the calculation of energy are performed via LABVIEW program with the help of Ni-cDAQ model NI-9174, two input modules model NI-9263 and one output module model NI-9234. A NI-cRIO controller model NI-9004 with one NI-9263 input module and one NI-9234 output module embedded with an FPGA-coded controller program is used to actively control the plate's vibration. Figures. 7(a) and 7(b) show experimental setup and interconnection diagram, respectively.

### A. OPTIMAL SENSOR-ACTUATOR LOCATION

This section aims to experimentally gauge the performance of the optimal parameters found in Section 4. Recall that the optimal parameters found theoretically are $x_{sa} = 0.3511$, $y_{sa} = 0.4550$, $K_p = 990$, $k_i = 210$ and $k_d = 19.88$. Fifteen natural frequencies are detected for less than 200 Hz, as shown in Table 8, compared to twelve natural frequencies found in the simulation. This is due to the placement of accelerometers on the plate, which consequently affected the plate's mass distribution and created another three natural frequencies, i.e., at 31.85 Hz, 57.5 Hz and 99.78 Hz. A significant reduction in acceleration measured by each accelerometer can be seen in Figure 8 and Table 9.

The following steps are taken to estimate the plate energy:

i Divide the plate into 8 divisions and place an accelerometer at the center of each division.

ii Calculate each plate division's kinetic energy separately by considering the mass of each division with the sensor and velocity sensed by each accelerometer. The total energy is the summation of energy for each division. Figure. 8 shows the comparison of energy generated between uncontrolled and controlled system while the corresponding reduction levels measured at each mode is given in Figures 9(a) and 9(b).

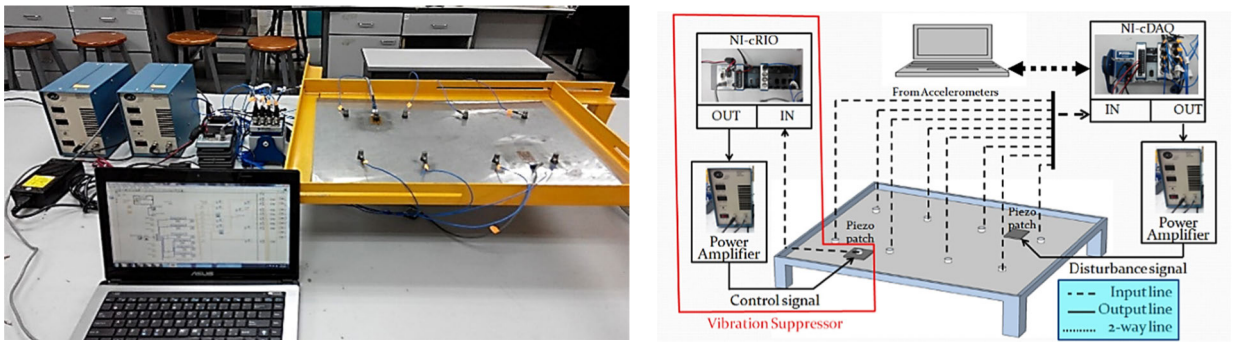


(a) (b)

**FIGURE 7.** (a) Experimental setup, and (b) Interconnection diagram.

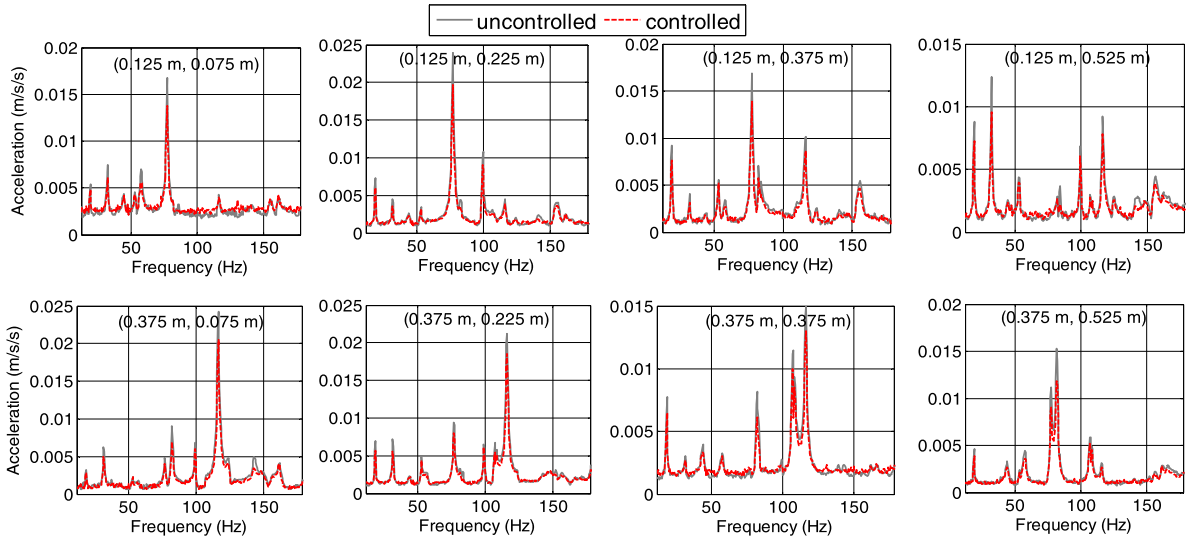


**FIGURE 8.** Acceleration signals calculated at each accelerometer.

**TABLE 8.** Experimental resonant frequencies (for below 200 Hz).

| Mode | Frequency (Hz) |
|---|---|
| 1 | 19.02 |
| 2 | 31.85 |
| 3 | 44.2 |
| 4 | 52.75 |
| 5 | 57.5 |
| 6 | 76.97 |
| 7 | 81.72 |
| 8 | 99.78 |
| 9 | 107.4 |
| 10 | 116.4 |
| 11 | 143.0 |
| 12 | 155.8 |
| 13 | 161.5 |
| 14 | 180.1 |
| 15 | 192.9 |

The frequency-averaged energy reduction achieved is 19.52%, which is slightly lower compared to the simulation result.

**TABLE 9.** Experimental results.

| Mode | Frequency (Hz) |
|---|---|
| 1st | 30.41 |
| 2nd | 38.02 |
| 3rd | 27.66 |
| 4th | 12.53 |
| 5th | 31.39 |
| Frequency averaged | 19.52 |

The frequency response of a continuous structure vibration is generally grouped into low, mid and high frequencies, based on the modal overlapping factor (MOF). Low-frequency response is deterministic, which exhibits distinct individual modes and is not sensitive to structural uncertainties (i.e., a small variation in mass or stiffness matrices) [34], [35].

In this current article, the work is performed within the low-frequency regions. The total mass of the accelerometers and portion of cables on the plate are considered small, and their effect on the low-frequency modes is insignificant.

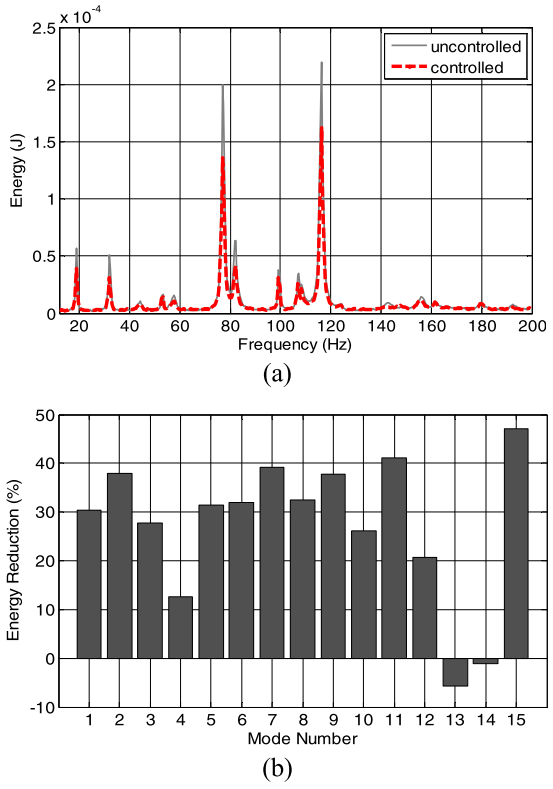


**FIGURE 9.** Experimental result for plate (a) energy and (b) energy reduction for each mode.

## VI. CONCLUSION

In this work, the ACO technique was utilized to optimise collocated sensor-actuator location on the flexible structure and obtain the optimal PID controller gains. The optimal values obtained from ACO are found comparable to the results from GA and the enumerative method. Based on the results, the PID controller gains and collocated sensor-actuator location optimizations using ACO, GA and enumerative methods give similar results. This implies the effectiveness of ACO for such optimization problems. The best location to place a collocated sensor-actuator to achieve the highest reduction of plate energy (or reduction of displacement for the whole plate) is near the exciter patch with more than 10% frequency-averaged energy reduction. This is because the highest energy reduction can be achieved by directly locking the disturbance force. However, in reality, the information about the disturbance such as magnitude and location is inaccessible. Since the location that causes vibration, and its corresponding magnitude can be difficult to identify. Hence, optimal location is investigated by setting at least 0.1 m gabs, along x and y axes, between excitation and sensor-actuator locations. As for the PID gains, with the PID controller gains been capped due to the output module's limitation (NI-9263) to produce voltage with the range of -10V to 10V only, about 20% of frequency-averaged energy reduction is achieved. A much better reduction would be accomplished if higher gains, or a better amplifier were used.

## ACKNOWLEDGMENT

Open Access funding has been provided by the Qatar National Library, Qatar.

## REFERENCES

[1] P. Wang, A. Korniienko, X. Bombois, M. Collet, G. Scorletti, E. Skow, C. Wang, and K. Colin, "Active vibration control in specific zones of smart structures," *Control Eng. Pract.*, vol. 84, pp. 305–322, Mar. 2019.

[2] M. R. Kermani, M. Moallem, and R. V. Patel, "Parameter selection and control design for vibration suppression using piezoelectric transducers," *Control Eng. Pract.*, vol. 12, no. 8, pp. 1005–1015, Aug. 2004.

[3] D. Halim and S. O. Reza Moheimani, "An optimization approach to optimal placement of collocated piezoelectric actuators and sensors on a thin plate," *Mechatronics*, vol. 13, no. 1, pp. 27–47, Feb. 2003.

[4] G. Caruso, S. Galeani, and L. Menini, "On actuators/sensors placement for collocated flexible plates," in *Proc. Medit. Conf. Control Automat.*, 2003.

[5] H. Si, D. Li, Z. Liu, and J. Liang, "Optimization of the number and locations of the actuators in smart structures," in *Proc. IEEE Int. Conf. Robot., Intell. Syst. Signal Process.*, Oct. 2003, pp. 841–846.

[6] I. Bruant and L. Proslier, "Optimal location of actuators and sensors in active vibration control," *J. Intell. Mater. Syst. Struct.*, vol. 16, no. 3, pp. 197–206, Mar. 2005.

[7] K. Ramesh Kumar and S. Narayanan, "The optimal location of piezoelectric actuators and sensors for vibration control of plates," *Smart Mater. Struct.*, vol. 16, no. 6, pp. 2680–2691, Dec. 2007.

[8] N. Darivandi, K. Morris, and A. Khajepour, "An algorithm for LQ optimal actuator location," *Smart Mater. Struct.*, vol. 22, no. 3, Mar. 2013, Art. no. 035001.

[9] X. Liu, G. Cai, F. Peng, and H. Zhang, "Piezoelectric actuator placement optimization and active vibration control of a membrane structure," *Acta Mechanica Solida Sinica*, vol. 31, no. 1, pp. 66–79, Feb. 2018.

[10] D. Piron, S. Pathak, A. Deraemaeker, and C. Collette, "A pole-zero based criterion for optimal placement of collocated sensor-actuator pair," *Mech. Syst. Signal Process.*, vol. 155, Jun. 2021, Art. no. 107533.

[11] S. Cantero-Chinchilla, J. L. Beck, M. Chiachío, J. Chiachío, D. Chronopoulos, and A. Jones, "Optimal sensor and actuator placement for structural health monitoring via an efficient convex cost-benefit optimization," *Mech. Syst. Signal Process.*, vol. 144, Oct. 2020, Art. no. 106901.

[12] T. L. da Rocha, S. Silva, and V. Lopes, "Optimal location of piezoelectric sensor and actuator for flexible structures," in *Proc. 11th Int. Congr. Sound Vib.*, 2004, pp. 1–8.

[13] J. Hu, X. Zhang, and Z. Kang, "Layout design of piezoelectric patches in structural linear quadratic regulator optimal control using topology optimization," *J. Intell. Mater. Syst. Struct.*, vol. 29, no. 10, pp. 2277–2294, Jun. 2018.

[14] M. A. Demetriou, "A numerical algorithm for the optimal placement of actuators and sensors for flexible structures," in *Proc. Amer. Control Conf.*, vol. 4, Jun. 2000, pp. 2290–2294.

[15] S. Julai, M. O. Tokhi, M. Mohamad, and I. A. Latiff, "Active vibration control of a flexible plate structure using particle swarm optimization," in *Proc. IEEE 9th Int. Conf. Cyberntic Intell. Syst.*, Sep. 2010, pp. 1–6.

[16] H. L. Ji, J. H. Qiu, Y. P. Wu, J. Cheng, and M. N. Ichchou, "Novel approach of self-sensing actuation for active vibration control," *J. Intell. Mater. Syst. Struct.*, vol. 22, no. 5, pp. 449–459, Mar. 2011.

[17] J.-H. Han and I. Lee, "Optimal placement of piezoelectric sensors and actuators for vibration control of a composite plate using genetic algorithms," *Smart Mater. Struct.*, vol. 8, no. 2, pp. 257–267, Apr. 1999.

[18] A. G. A. Muthalif and R. S. Langley, "Active control of high-frequency vibration: Optimisation using the hybrid modelling method," *J. Sound Vib.*, vol. 331, no. 13, pp. 2969–2983, Jun. 2012.

[19] P. Wang and D. P. Kwok, "Optimal design of PID process controllers based on genetic algorithms," *Control Eng. Pract.*, vol. 2, no. 4, pp. 641–648, Aug. 1994.

[20] M. Karami, A. R. Tavakolpour-Saleh, and A. Norouzi, "Optimal nonlinear PID control of a micro-robot equipped with vibratory actuator using ant colony algorithm: Simulation and experiment," *J. Intell. Robotic Syst.*, vol. 99, nos. 3–4, pp. 773–796, Sep. 2020.

[21] I. Chiha, N. Liouane, and P. Borne, "Tuning PID controller using multiobjective ant colony optimization," *Appl. Comput. Intell. Soft Comput.*, vol. 2012, pp. 1–7, Jan. 2012.

[22] H. Nobahari, S. A. H. Kordkheili, and S. S. Afshari, "Hardware-in-the-loop optimization of an active vibration controller in a flexible beam structure using evolutionary algorithms," *J. Intell. Mater. Syst. Struct.*, vol. 25, no. 10, pp. 1211–1223, Sep. 2014.
[23] M. Mohamad, M. O. Tokhi, and M. Omar, "Continuous ant colony optimisation for active vibration control of flexible beam structures," in *Proc. IEEE Int. Conf. Mechatronics*, Apr. 2011, pp. 803–808.
[24] A. Preumont, "Vibration control of active structures," in *Solid Mechanics and Its Applications*, vol. 179. Cham, Switzerland: Springer, 2011, pp. 1–452.
[25] S. Timoshenko and S. Woinowsky-Krieger, *Theory of Plates and shells*. New York, NY, USA: McGraw-Hill, 1959.
[26] P. Mehta, "Vibrations of thin plate with piezoelectric actuator: Theory and experiments," M.S. thesis, Dept. Mech. Eng., Clemson Univ., Clemson, SC, USA, Dec. 2009.
[27] A. G. A. Muthalif, A. N. Wahid, and K. A. M. Nor, "Estimating ensemble average power delivered by a piezoelectric patch actuator to a non-deterministic subsystem," *J. Sound Vib.*, vol. 333, no. 4, pp. 1149–1162, Feb. 2014.
[28] M. Jalili-Kharaajoo, B. Moshiri, K. Shabani, and H. Ebrahimirad, "Genetic algorithm based parameter tuning of adaptive LQR-repetitive controllers with application to uninterruptible power supply systems," in *Innovations in Applied Artificial Intelligence* (Lecture Notes in Computer Science), vol. 3029, B. Orchard, C. Yang, and M. Ali, Eds. Berlin, Germany: Springer, 2004, doi: 10.1007/978-3-540-24677-0_60.
[29] F. Peng, A. Ng, and Y.-R. Hu, "Actuator placement optimization and adaptive vibration control of plate smart structures," *J. Intell. Mater. Syst. Struct.*, vol. 16, no. 3, pp. 263–271, Mar. 2005.
[30] J. Li and W. Li, "On-line PID parameters optimization control for wind power generation system based on genetic algorithm," *IEEE Access*, vol. 8, pp. 137094–137100, 2020.
[31] M. E. C. Bento, D. Dotta, R. Kuiava, and R. A. Ramos, "A procedure to design fault-tolerant wide-area damping controllers," *IEEE Access*, vol. 6, pp. 23383–23405, Apr. 2018.
[32] J. Wan, B. He, D. Wang, T. Yan, and Y. Shen, "Fractional-order PID motion control for AUV using cloud-model-based quantum genetic algorithm," *IEEE Access*, vol. 7, pp. 124828–124843, 2019.
[33] F. Meng, S. Liu, and K. Liu, "Design of an optimal fractional order PID for constant tension control system," *IEEE Access*, vol. 8, pp. 58933–58939, 2020.
[34] A. G. A. Muthalif and A. N. Wahid, "Optimal piezoelectric shunt dampers for non-deterministic substructure vibration control: Estimation and parametric investigation," *Sci. Rep.*, vol. 11, no. 1, p. 4642, Dec. 2021.
[35] A. Ali, A. G. A. Muthalif, and J. Renno, "Broadband vibration energy harvesting from a non-deterministic system: Performance of different piezoelectric patch shapes," *Mater. Res. Exp.*, vol. 8, no. 2, Feb. 2021, Art. no. 025702.

**ASAN G. A. MUTHALIF** (Senior Member, IEEE) received the bachelor's and master's degrees in mechatronics engineering from International Islamic University Malaysia (IIUM) and the Ph.D. degree from Cambridge University, U.K., in 2008. He is currently an Associate Professor with the Department of Mechanical and Industrial Engineering, Qatar University. His research interests include mechatronics, active and semi-active vibration control, smart materials and structures, vibration-based energy harvesting, mid-high frequency vibration control, statistical energy analysis (SEA), and dynamics of built-up structures.

**KHAIRUL A. M. NOR** received the bachelor's and master's degrees in mechatronics engineering from International Islamic University Malaysia (IIUM), and the Ph.D. degree from The University of Auckland, New Zealand, in 2019. He is currently an Assistant Professor with the Department of Mechatronics Engineering, IIUM. His research interests include vibration control, active noise cancellation, active structural acoustic control, adaptive control, and vibration-based energy harvesting.

**AZNI NABELA WAHID** received the B.Eng. degree in mechanical engineering from Vanderbilt University, USA, and the M.Sc. degree in mechatronics engineering and the Ph.D. degree in engineering from International Islamic University Malaysia. She is currently working as an Assistant Professor with the Department of Mechatronics Engineering, International Islamic University Malaysia. Her research interests include vibration analysis and control, energy harvesting, and smart materials.

**ABDELRAHMAN ALI** received the bachelor's degree in mechanical engineering from Qatar University, Doha, Qatar, in 2020, where he is currently pursuing the master's degree in mechanical engineering. He is also working as a Research Assistant with the Mechanical and Industrial Engineering Department. His research interests include active and semi-active vibration control, piezoelectric vibration energy harvesting, smart materials and structures (magnetorheological elastomers and fluids), and finite element analysis.